THE ASTROPHYSICAL JOURNAL, 465:L141–L144, 1996 July 10

MEASUREMENT OF HYDROGEN VELOCITY DISTRIBUTIONS IN THE EXTENDED SOLAR CORONA

J. L. KOHL, L. STRACHAN, AND L. D. GARDNER
Harvard-Smithsonian Center for Astrophysics, Cambridge, MA 02138
Received 1996 March 8; accepted 1996 May 3

ABSTRACT

H I Lyα spectral line profiles have been measured in polar regions of the solar corona at projected heliocentric heights of 1.8–3.5 $R_\odot$. Observations were made with the Ultraviolet Coronal Spectrometer on the *Spartan 201* satellite from 16:52 to 04:04 UT on 1993 April 11–12 (south pole) and from 12:28 to 22:09 UT on 1993 April 12 (north pole). In general, the coronal profiles cannot be accurately curve-fitted with a single-Gaussian function. The fits with two Gaussians yield most probable velocities of 158 and 322 km s^{-1} (south) and 98 and 266 km s^{-1} (north). These parameters vary by less than 10% (1 σ) over the observed heights.

The observations are consistent with a line-of-sight model that attributes the narrow component to background streamers and to sites within polar coronal holes or a surrounding diffuse corona, and the broad component to the polar coronal holes and/or plumes. This interpretation suggests that there are regions within the observed coronal holes that have hydrogen and proton kinetic temperatures of (4–6) $\times$ 10^6 K, which is 4–10 times higher than the expected electron temperatures at the same heights. However, other models with, for example, local non-Maxwellian velocity distributions are also consistent with the observations.

Subject headings: solar wind — Sun: corona — Sun: UV radiation

1. INTRODUCTION

The spectral line profiles of H I Lyα in the extended solar corona provide a direct measurement of the velocity distribution of neutral hydrogen along the line of sight (LOS). Coronal H I Lyα is formed by resonant scattering of chromospheric H I Lyα by the small fraction of protons and electrons that exist as neutral H in the high-temperature corona (Gabriel 1971). For near 90° scattering, which tends to be the case for observations above the limb, the angular dependence of resonant scattering has only a small effect on the observed spectral line profiles (Withbroe et al. 1982). Hence, for precisions of $\pm$10%, the observed line profile can be converted to a velocity distribution using the usual Doppler shift formula:

$$\frac{\Delta\lambda}{\lambda_0} = \frac{V}{c}, \quad (1)$$

where $\Delta\lambda$ is the wavelength shift from the line center, λ_0, and c is the speed of light. Furthermore, the resulting H velocity distribution is believed to be representative of the coronal proton distribution (Withbroe et al. 1982; Leer 1988).

2. DESCRIPTION OF THE ULTRAVIOLET CORONAL SPECTROMETER/*SPARTAN 201* EXPERIMENT

The Spartan Ultraviolet Coronal Spectrometer is based on the design of a rocket instrument (Kohl, Reeves, & Kirkham 1978) and is described in Kohl, Gardner, & Strachan (1995). It is an externally and internally occulted reflecting telescope and a dual spectrometer. The telescope mirror used for H I Lyα has a 47.5 cm focal length and has an Al + MgF_2 coating. Mirror motions are used to scan radially from 1.5 to 3.5 $R_\odot$. An Ebert-Fastie spectrometer is used for H I Lyα. It has two entrance slits; one is 0.5 $\times$ 2.5 arcmin^2 to measure the line profile, and the other is 4.0 $\times$ 5.0 arcmin^2 to measure the total line intensity. The detector is a discrete anode microchannel array (Timothy, Mount, & Bybee 1981) with 48 pixels to measure the line profile with 0.25 Å spectral elements and 42 pixels to measure the line intensity with 2.0 Å spectral elements.

3. OBSERVATIONS

At the time of the observations, coronal holes at the north and south poles were dominant, long-lasting features in the corona. The electron densities and geometry of these structures, as determined by the Spartan White Light Coronagraph, have been described by Fisher & Guhathakurta (1995).

South polar region observations were made from 16:52 to 04:04 UT on 1993 April 11–12. In the following, we present profile measurements at several position angles starting at a projected heliocentric height (in $R_\odot$) of ρ = 1.83 and stepping out in height up to a maximum of ρ = 2.53. Four position angles separated by 10° and centered on the south coronal hole were observed. North polar region observations were made from 12:28 to 22:09 UT on 1993 April 12. Profile measurements were made along three position angles separated by 10°. An observation was also made in the north at ρ = 3.52.

Figure 1*c* shows the H I Lyα profile obtained at ρ = 3.52 in the north polar region. The data points show counts in each 0.25 Å resolution bin of the detector. The error bars indicate the $\pm$1 σ uncertainties in the data (see § 4). A prominent feature of this profile is the narrow geocoronal component near the center of the profile. This feature is due to solar H I Lyα that undergoes resonant scattering by the neutral H in the atmospheric layers above *Spartan 201*'s orbit. The actual width of the geocoronal line is only 0.02 Å, but this is broadened by the instrument profile function. Figure 1*c* also demonstrates that the scattered light is negligible, since there is no component with the width of the chromospheric H I Lyα (Kohl et al. 1994).

Examples of other profiles from the north polar region are shown in Figures 1*a* and 1*b* and Figure 2*a*. In all cases the narrow geocoronal component has been removed. For comparison, a sample profile from the south polar region is shown

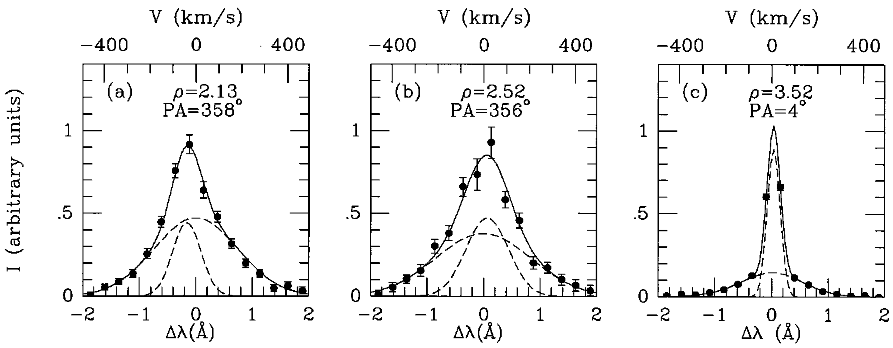

FIG. 1.—H I Lyα profiles from the north polar region showing 1 σ uncertainties in the data. Dashed curves in (*a*) and (*b*) are Gaussian components of the total coronal profile (*solid curve*). In (*c*) the two dashed components are the total coronal and net geocoronal contributions. The geocoronal contribution has been removed from the profiles in (*a*) and (*b*).

in Figure 2*b*. Both north and south profiles have extended wings with narrow profile cores.

4. DATA REDUCTION

The profiles in Figures 1 and 2 have been corrected for background counts and detector nonuniformities. The detector background was determined by averaging the pixel counts detected when *Spartan 201* was in the Earth's umbra and looking toward the Earth. A small exospheric contribution was subtracted from these measurements. The background correction is normally very small compared to the total counts in each pixel. After the background correction, the profile is corrected for detector cross-talk. This correction is based on laboratory measurements which have been shown to be constant during the time between the preflight and postflight calibrations. Approximately 2×10^{-3} of the peak counts in the intensity channel were subtracted from the counts in each pixel of the profile channel. The actual correction is different for each pixel. No artificial baseline correction has been made to force the wings of the profiles to go to zero. Nonetheless, the profile wings fall off to zero, which indicates that the detector backgrounds and corrections are well understood. Each profile also has been flat-field–corrected for the slightly different sensitivities of each pixel. This correction removes most of the unevenness in the distribution of the data, except for the irregularity that appears near the peak of some of the profiles.

5. PROFILE FITS

The profiles in Figures 1*a* and 1*b* and in Figures 2*a* and 2*b* are shown without the narrow geocoronal component. To remove this component, the observed profiles were fitted with three Gaussian curves, one of which was constrained to have the $1/e$ half-width of the instrument profile (0.16 Å). The wavelength position of that component, attributed to the geocorona, is known from Figure 1*c* and the known spacecraft velocity. This component accounts for both geocoronal emission and the absorption of coronal radiation by exospheric hydrogen.

Two Gaussians were used to fit the coronal profile, depending on goodness of fit. Goodness of fit was subjective but was determined by minimizing the χ^2 of the residuals at each data point. No constraints were made on the amplitude, width, or central-wavelength offset of the coronal Gaussians.

Figures 1 and 2 illustrate the curve fits for several representative profiles and also include the conversion of the wavelength scale to velocity using equation (1). We have used the streamer profile in Figure 2*c*, which has a single-Gaussian shape, to verify that the instrument profile cannot account for the enhanced line wings of the coronal hole profiles. Table 1 gives the parameters for these and other profiles observed in both polar coronal regions. I_{tot} is the total profile integrated intensity and I_B/I_{tot} is the ratio of the integrated intensity for the broad component to that of the total intensity. The most probable velocities, V_{mp}, for the narrow and broad profiles are in the columns labeled V_N and V_B. V_{mp} is the velocity where the profile (after being deconvolved from the instrument profile) is at $1/e$ of the maximum amplitude. The columns labeled ΔV_N and ΔV_B refer to equivalent velocity shifts of the profile components. All velocities have been corrected for the spacecraft orbital motion.

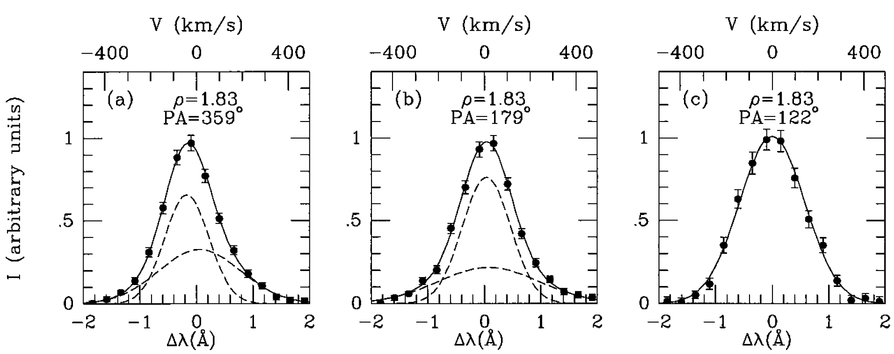

FIG. 2.—H I Lyα profiles from (*a*) the north polar region, (*b*) the south polar region, and (*c*) a helmet streamer. Dashed curves are Gaussian components to the total profile fit (*solid curve*). Note that the streamer profile data is fitted with a single Gaussian. The geocoronal contribution has been removed from all profiles.

TABLE 1

Spartan 201-1 H I Lyα Profile Parameters

Height ($R_\odot$)	P.A. (deg)	I_{tot} (photons s^{-1} cm^{-2} sr^{-1})	I_B/I_{tot}	V_N (km s^{-1})	ΔV_N (km s^{-1})	V_B (km s^{-1})	ΔV_B (km s^{-1})
North Polar Region							
1.83	349.3	2.91×10^{10}	0.887	73	−36	196	−13
1.83	359.3	4.89×10^{10}	0.478	132	−41	250	14
1.83	9.3	3.99×10^{10}	0.459	130	−21	285	−6.6
Average	...	3.93×10^{10}	0.608	112	−33	244	−1.9
2.13	347.9	1.12×10^{10}	0.714	92	−23	327	−17
2.13	357.9	1.11×10^{10}	0.758	78	−44	255	−5
2.13	7.9	3.09×10^{10}	0.732	99	−20	223	−4.3
Average	...	1.77×10^{10}	0.735	90	−29	268	−8.8
2.52	346.5	2.29×10^{10}	0.832	75	−52	326	−9.6
2.52	356.5	7.27×10^{9}	0.642	125	11	292	−6.7
Average	...	1.51×10^{10}	0.737	100	−20	309	−8.2
3.52	4.3	1.65×10^{9}	0.653	92	−5.4	243	−13
South Polar Region							
1.73	189.9	4.34×10^{10}	0.336	147	0.3	330	12
1.83	179.3	2.39×10^{10}	0.375	144	10	312	20
1.83	189.3	2.46×10^{10}	0.231	163	4.5	353	−26
1.83	199.3	2.37×10^{10}	0.272	162	19	355	36
1.83	209.3	3.38×10^{10}	0.349	144	22	316	9.7
Average	...	2.65×10^{10}	0.307	153	14	334	9.9
2.13	177.9	6.93×10^{9}	0.416	188	25	511	30
2.13	187.9	7.04×10^{9}	0.516	169	18	275	−4.6
2.13	207.9	6.24×10^{9}	0.804	145	2.3	219	43
Average	...	6.74×10^{9}	0.579	167	15	335	23
2.52	186.5	1.93×10^{9}	0.525	170	−22	275	75
2.52	206.5	2.52×10^{9}	0.658	157	24	301	39
Average	...	2.23×10^{9}	0.592	164	1	288	57

6. DISCUSSION

It is clear that the velocity distribution along the LOS in the polar regions is not a single Gaussian as might be expected for an approximately isothermal LOS. Instead we find a coronal profile that is well fitted to two Gaussians after backgrounds and a geocoronal contribution are removed. If we average the V_{mp}'s for each component at each height, we find little variation with height. For the north polar region the narrow (broad) component has an average value of 98 km s^{-1} (266 km s^{-1}), corresponding to 5.8×10^5 K (4.3×10^6 K), and for the south polar region the narrow (broad) component has an average value of 158 km s^{-1} (322 km s^{-1}), corresponding to 1.51×10^6 K (6.28×10^6 K) for all observed heights.

The observed H I Lyα profiles suggest either a coronal plasma with sites along the LOS that have very different kinetic temperatures or a plasma with local non-Maxwellian velocity distributions. In the following, we discuss examples of each case and their consistency with the observations.

An example of the first case, discussed by Axford (1995), is that the LOSs through the polar corona have contributions from three sites: the tips of high-latitude helmet streamers, a diffuse corona adjacent to polar coronal holes, and the coronal holes themselves, including polar plumes. The contribution from streamers to the south polar region observations can be estimated from H I Lyα observations of a streamer that was above the southeast limb at position angle 131° at the time of the observations. This streamer appears to follow a neutral line that extends from Carrington longitude −180° to +30° (Real 1993). Observations with the Mark III coronagraph on Mauna Loa indicate that streamers at the approximate latitude of this streamer were present near the plane of the sky for at least a half-rotation before and after the *Spartan 201* observations. It appears that the streamer nearly encircles the Sun, and is shaped like an archway along the observed neutral line.

Spartan 201 white-light images (Fisher & Guhathakurta 1994) of the streamer indicate that it is not radial. A streamer archway with the observed orientation would be expected to intersect the LOS for the H I Lyα observation for $\rho = 1.83$ at about 3.5 $R_\odot$ in the background but not the foreground. The V_{mp} and intensity of the streamer at 3.5 $R_\odot$ were determined by the Spartan Ultraviolet Coronal Spectrometer (Strachan et al. 1994) to be V_{mp} = 190 km s^{-1} and $I = 8.6 \times 10^9$ photons s^{-1} cm^{-2} sr^{-1}.

The average value of V_{mp} for the narrow component in the south polar region at $\rho = 1.83$ is 153 km s^{-1}. The difference from the streamer value at 3.5 $R_\odot$ might be explained by another contribution to the narrow component, such as the coronal hole or a diffuse corona surrounding the coronal hole. It can be seen from Table 1 that the average intensity of the narrow component at $\rho = 1.83$ in the south is 1.84×10^{10} photons s^{-1} cm^{-2} sr^{-1}. This is approximately twice the intensity of the streamer at the intersection point. The larger observed intensity is further evidence of another contributor to the narrow component.

In the case of the north polar region, there are no high-latitude streamers with intensities approaching that of the ones in the south. The fact that the broad component is a larger fraction of the total intensity in the north is consistent with the absence of bright streamers. The value of V_{mp} for the narrow component is significantly smaller than for the south hole at all observed heights.

As mentioned above, the narrow component of the two-Gaussian fits may be attributable to several sites. In at least the south polar region, streamers appear to contribute about half of the observed intensity, but have a larger line width than is observed. The remainder of the narrow component may have a width similar to that observed in the narrow component of the north polar region. It could be formed in the coronal hole itself or in the diffuse corona. We are left with the broad component being attributed to the coronal hole and/or plumes with a kinetic temperature of 4–10 times the expected electron temperature (Habbal, Esser, & Arndt 1993). Hence, the observations are consistent with mechanisms discussed by McKenzie, Banaszkiewicz, & Axford (1995) that preferentially heat particles in proportion to their mass.

It appears that explanations with a local non-Maxwellian velocity distribution do not account, at least, for the streamer contribution to the south hole. However, the coronal hole contribution could result from a combination of thermal velocities and transverse wave motions (Leer 1988). There also could be some contribution from nonradial outflows. Scudder (1992) has described mechanisms for producing non-Maxwellian distributions in low-density plasmas.

The velocity shifts in Table 1 suggest that the narrow and broad components correspond to different outflows and, therefore, have different origins. In the south polar region the narrow profile components show small LOS velocities which are not distinct from zero within the scatter of the data. The fact that the LOS velocities are small further supports the idea that the narrow component is due, in part, to the background streamer arcade, which is expected to have a low outflow velocity. (The small positive mean LOS values may be due to the fact that some of the intensity in the narrow component is due to material in the coronal hole itself.) The hot material in the south polar region (responsible for the broad profile) has LOS velocity components whose mean value increases steadily with height and, hence, appears to be associated with outflows from the coronal hole.

The hot sites in the north coronal hole have mean LOS velocity shifts that are small and negative but essentially zero. This implies that those hot sites have outflows with nearly equal amounts of material flowing forward and backward along the LOS. The large negative shifts of the narrow profile component may be due to cooler sites in the coronal hole that are moving toward the observer. This is consistent with the idea that some of the narrow component comes from sites in the coronal hole that contribute to the solar wind but are distinct from the sites that form the broad component.

The authors wish to thank D. Daugherty for assistance in reducing the flight profile data. This work was supported by NASA under grant NAG5-613 to the Smithsonian Astrophysical Observatory.

REFERENCES

Axford, W. I. 1995, private communication
Fisher, R. R., & Guhathakurta, M. 1994, Space Sci. Rev., 70, 267
———. 1995, ApJ, 447, L139
Gabriel, A. H. 1971, Sol. Phys., 21, 392
Habbal, S. R., Esser, R., & Arndt, M. B. 1993, ApJ, 413, 435
Kohl, J. L., Reeves, E. M., & Kirkham, B. 1978, in New Instrumentation for Space Astronomy, ed. K. A. van der Hucht & G. Vaiana (New York: Pergamon), 91
Kohl, J. L., Gardner, L. D., Strachan, L., & Hassler, D. M. 1994, Space Sci. Rev., 70, 253
Kohl, J. L., Gardner, L. D., & Strachan, L. 1995, Space Sci. Rev., 72, 29
Leer, E. 1988, in Proc. Sixth Int. Solar Wind Conf., ed. V. J. Pizzo, T. E. Holzer, & D. G. Sime (NCAR/TN-306+Proc.; Boulder: NCAR), 89
McKenzie, J. F., Banaszkiewicz, M., & Axford, W. I. 1995, A&A, 303, L45
Real, D. 1993, Prelim. Report Sol. Geophys. Data (SESC PRF 919; Boulder: NOAA-USAF/SESC), 22
Scudder, J. D. 1992, ApJ, 398, 319
Strachan, L., Gardner, L. D., Hassler, D. M., & Kohl, J. L. 1994, Space Sci. Rev., 70, 263
Timothy, J. G., Mount, G. H., & Bybee, R. L. 1981, IEEE Trans. Nucl. Sci., NS-28, 689
Withbroe, G. L., Kohl, J. L., Weiser, H., & Munro, R. H. 1982, Space Sci. Rev., 33, 17